

OPEN ACCESS

EDITED BY

Venkata Satya Siva Srikanth Vadali, University of Hyderabad, India

REVIEWED BY

Pandiyarajan Thangaraj, Indian Institute of Information Technology Design and Manufacturing, Kurnool, India Shankar Muthukonda Venkatakrishnan, Yogi Vemana University, India

*CORRESPONDENCE

Y. Prashanthi.

□ dryprasanthi@gmail.com

Parameswaram Ganji,

☑ Parameswaram.ganji@ijs.si

RECEIVED 28 July 2025
ACCEPTED 26 September 2025
PUBLISHED 17 October 2025

CITATION

Pamula UP, Rao TN, Prashanthi Y and Ganji P (2025) Synthesis and characterization of ZnO@ CTAB-SA polymer nanocomposites with biological and photocatalytic activity. Front. Nanotechnol. 7:1674700. doi: 10.3389/fnano.2025.1674700

COPYRIGHT

© 2025 Pamula, Rao, Prashanthi and Ganji. This is an open-access article distributed under the terms of the Creative Commons Attribution License (CC BY). The use, distribution or reproduction in other forums is permitted, provided the original author(s) and the copyright owner(s) are credited and that the original publication in this journal is cited, in accordance with accepted academic practice. No use, distribution or reproduction is permitted which does not comply with these terms.

Synthesis and characterization of ZnO@CTAB-SA polymer nanocomposites with biological and photocatalytic activity

Uday Prakash Pamula¹, Tentu Nageswara Rao², Y. Prashanthi¹* and Parameswaram Ganji³*

¹Department of Chemistry, Mahatma Gandhi University, Nalgonda, Telangana, India, ²Department of Analytical Chemistry, Isosphere Biosciences Pvt Ltd., Secundrabad, Telangana, India, ³Department of Surface Engineering, Jožef Stefan Institute, Ljubljana, Slovenia

Aim: This study explores the synthesis and characterization of ZnO-based polymer nanocomposites (ZnO@CTAB-SA) employing sodium alginate (SA) and cetyltrimethylammonium bromide (CTAB) as matrices.

Material and Methods: The composites were synthesized using an *in-situ* polymerization method, integrating different amounts of ZnO nanoparticles. The materials exhibited substantial antibacterial effectiveness against *Staphylococcus aureus* (Gram-positive) and *Escherichia coli* (Gram-negative), in addition to antifungal activity against *Aspergillus niger*. Characterization methods including FTIR, PXRD, SEM, and EDAX validated the structural integrity and efficient dispersion of ZnO nanoparticles within the polymer matrix. Furthermore, the composites demonstrated improved photocatalytic degradation of commercial dyes, such as Rhodamine B and Alizarin Red S, facilitated by adsorption and surface contacts.

Results and Discussion: These results exhibit ZnO@CTAB-SA nanocomposites as a promising multifunctional material for biomedical antibacterial approaches. **Conclusion:** CTAB and ZnO nanoparticles enhance the composite structure and microbial cell contact, leading to increased bioactivity. These nanocomposites effectively degrade commercial dyes like Rhodamine B and Alizarin Red S through photocatalysis, indicating their potential for wastewater treatment.

KEYWORDS

zinc oxide polymer nanocomposites, sodium alginate (SA) cetyltrimethylammonium bromide (CTAB), antimicrobial activity, antifungal activity, and dye adsorption

1 Introduction

Nanocomposite materials are becoming increasingly popular due to their unique characteristics and a better understanding of nanoscale processes. The purpose of blending is to combine all polymers in the mixture to get the desired properties. Metal nanoparticles can serve as fillers to enhance sodium alginate's structural, optical, and electrical properties, yielding organic or inorganic composites. Nanoparticle materials produce polymeric nanocomposites with a significant surface area (Kapoor et al., 2017). Metal nanoparticles, particularly Ni/ZnO NPs (nickel and zinc oxide), are utilized throughout several industrial sectors, including chemical, optical, and electrical domains (Bao et al., 2011). Ni/ZnO nanoparticles augment antimicrobial coatings, nutritional supplements, food packaging, and medical equipment. Metal oxides are increasingly

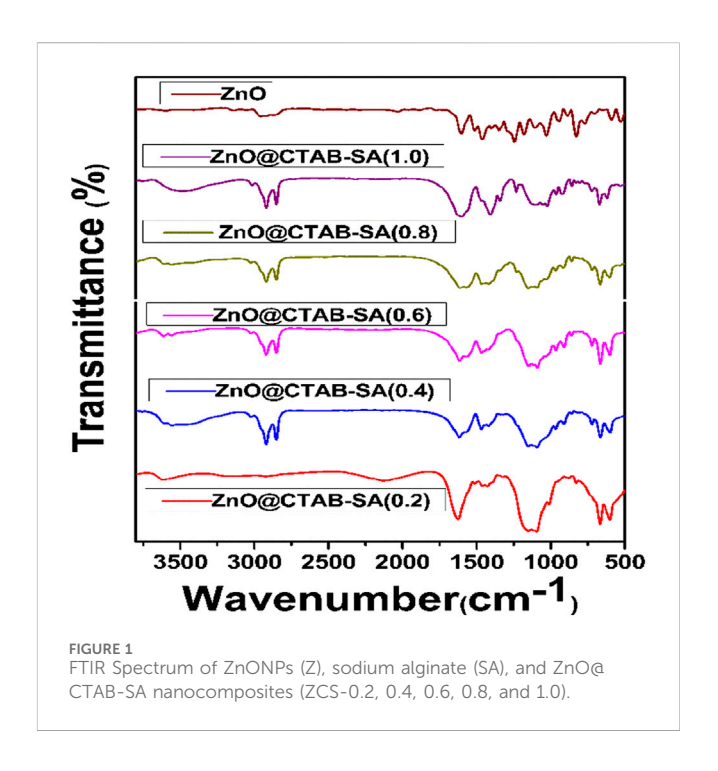
TABLE 1 Sample codes and descriptions of pure ZnO nanoparticles and ZnO@CTAB-SA polymer nanocomposites with varying ZnO contents.

Sample ID	Code	Description
ZnO NCs	Z	Pure ZnO nanoparticles
ZnO@CTAB-SA (0.2)	ZCS-(0.2)	Nanocomposite containing 10 wt% ZnO with CTAB-SA
ZnO@CTAB-SA (0.4)	ZCS-(0.4)	Nanocomposite containing 20 wt% ZnO with CTAB-SA
ZnO@CTAB-SA (0.6)	ZCS-(0.6)	Nanocomposite containing 30 wt% ZnO with CTAB-SA
ZnO@CTAB-SA (0.8)	ZCS-(0.8)	Nanocomposite containing 40 wt% ZnO with CTAB-SA
ZnO@CTAB-SA (1.0)	ZCS-(1.0)	Nanocomposite containing 50 wt% ZnO with CTAB-SA

employed for antibacterial purposes because of their stability, durability, and longer shelf life than organic chemicals (Rezaei et al., 2024; Matijaković Mlinarić et al., 2024). Nanoparticles such as CeO₂, TiO₂, CuO, MgO, ZnO, CaO, Al₂O₃, and Ag₂O have demonstrated effectiveness against several bacterial strains, including *S aureus* and *E coli* (Demirel and Erol Taygun, 2023; Perfileva and Krutovsky, 2024; Devi et al., 2024; Sánchez-López et al., 2023; Ashhari et al., 2023; Izzi et al., 2023; Canama et al., 2023; Zhou et al., 2023).

It has been shown that TiO2 solutions may sterilize Staphylococcus aureus, and E. coli viruses when exposed to ultraviolet light (Hao et al., 2023; Manabolu Surya et al., 2025). Because ZnO nanoparticles are safe, non-toxic, and biocompatible, they can carry drugs, make cosmetics, and make medical materials (Paul et al., 2023; Valinton et al., 2022; Garcia et al., 2022; Wu et al., 2022; Bains et al., 2022; Gharpure et al., 2022; Pandey et al., 2021). Some nanomaterials can hurt live cells, but Eukaryotic cells can usually handle low amounts of ZnO (Pandey et al., 2021; Hosseini et al., 2021; Yan et al., 2021a; Zhang et al., 2021; Zare et al., 2021). Polymers are widely employed as matrix components due to their low cost, processability, and versatility. While a lot of study has been done on structural polymer-based nanocomposites, not as much has been done on polymer nanocomposites for functional uses. For various reasons, including electrical conductivity, optical features, properties, and increased catalytic nanocomposites containing metal nanoparticles distributed inside a dielectric matrix are particularly interesting (Loomba et al., 2025; El-Samak et al., 2021; Yan et al., 2021b; Wee, 1998; Nallamalla

This is due to the fact that these nanocomposites have special qualities and can be used for various purposes. Because of its biocompatibility, low toxicity, cost-effectiveness, and gelation qualities with divalent cations like Ca2+, alginate—a naturally occurring anionic polymer made from brown seaweed is widely used in biomedical applications (Tabata, 2000). In the process of wound healing, controlled medicine administration, and cell transplantation, alginate hydrogels are utilized. These hydrogels duplicate the extracellular matrix. They maintain a hydrated wound environment, reduce infection risk, and they make it possible to administer a variety of drugs in a controlled manner. Pharmaceutical applications that include oral or injectable alginate gels are considered to be less invasive. Through the enhancement of cell transport and tissue creation, tissue engineering assists with the processes of cell transplantation and artificial tissue synthesis (Lee and Mooney, 2001). Cetyltrimethylammonium bromide, often



known as CTAB, is a cationic surfactant that is frequently used in the synthesis of nanoparticles to control the size and shape of the particles. Through the establishment of a stable interface between ZnO nanoparticles and the polymer matrix, CTAB has the potential to facilitate the overall production of homogeneous nanocomposites. Through the effective dispersion and stability of nanoparticles, it is envisaged that the synergistic integration of ZnO nanoparticles, sodium alginate, and CTAB in a polymer nanocomposite will enhance the effectiveness of antibacterial and antifungal agents (Ambalgi et al., 2016).

In addition to its relevance in biomedical and antimicrobial instances, the problem of dye pollution in water ecosystems has surfaced as a significant environmental concern. Dyes like Rhodamine B and Alizarin Red, two industrial dyes, have found widespread application in the textile, paper, and leather sectors, resulting in considerable water pollution. The toxicity of these dyes is significant, as they are non-biodegradable and threaten aquatic ecosystems and human health, leading to consequences (Nallamalla et al., 2025).

The present synthesis approach employs sodium alginate, a naturally occurring, biodegradable, and renewable polysaccharide

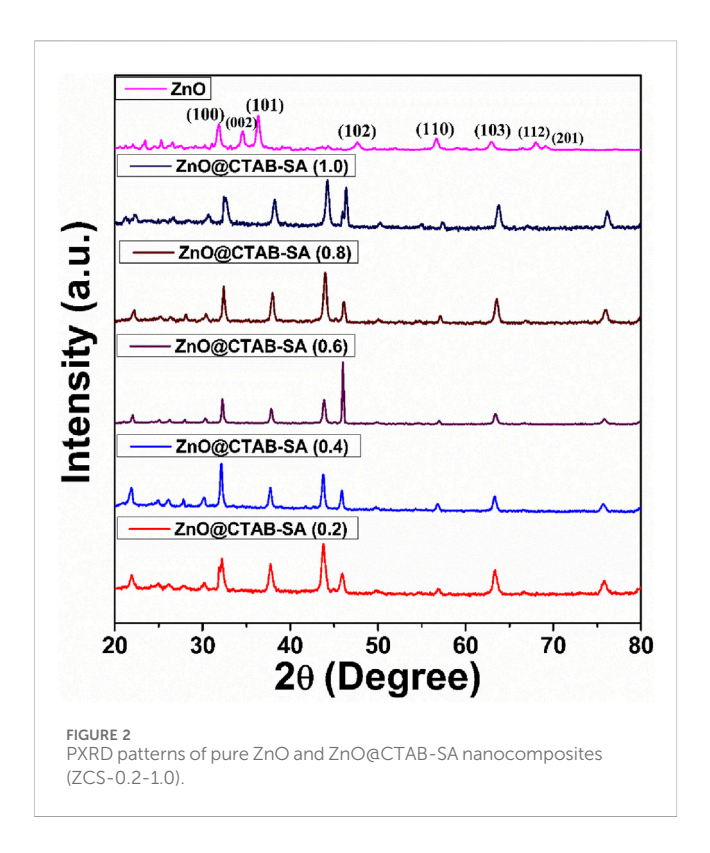


TABLE 2 PXRD peak assignment of ZnO (JCPDS 36-1,451).

hkl	Standard 2θ(°)	Observed 2θ(°)	D spacing (A°)
(100)	31.9	31.8	2.81
(002)	34.6	34.7	2.59
(101)	36.2	36.3	2.48
(102)	47.5	47.7	1.91
(110)	56.6	56.7	1.62
(103)	62.8	62.9	1.48
(200)	66.3	66.2	1.41
(112)	67.9	67.8	1.38
(201)	69.0	69.1	1.36

derived from seaweed, as the primary polymer matrix. The synthesis is carried out in aqueous and ethanol media, avoiding toxic or hazardous organic solvents, and the process conditions involve relatively low temperatures without the need for harsh reagents or catalysts. In addition, CTAB, used in controlled amounts, facilitates nanoparticle dispersion while remaining biodegradable. The resultant ZnO@CTAB-SA nanocomposites not only minimize the use of harmful chemicals during synthesis but also provide a sustainable solution for antimicrobial and wastewater treatment applications, thereby contributing to both environmental safety and green chemistry practices.

To address these challenges, polymer nanocomposites offer a promising solution due to their high surface area, tunable chemical properties, and enhanced interaction sites. The current study introduces polymer nanocomposites of ZnO nanoparticles, with sodium alginate, and CTAB as a viable solution to microbial, fungal resistance, and dye degradation. These synthesized nanocomposites demonstrate superior antibacterial and antifungal activity and efficiently adsorb dyes and degradation via synergetic surface adsorption and chemical interactions. Several studies have reported ZnO-polymer composites for antimicrobial and photocatalytic applications. However, the combined integration of ZnO with sodium alginate (a natural interaction) has been scarcely explored. This unique combination is expected to improve nanoparticle stabilization, enhance dye adsorption, and boost antimicrobial activity. To the best of our knowledge, the multifunctional ZnO@CTAB-SA nanocomposites reported here represent one of the first attempts to utilize this synergistic polymer-surfactant framework for both biomedical and environmental applications. Therefore, the present study focuses on the synthesis, characterization, and evaluation of ZnO@CTAB-SA nanocomposites for antimicrobial and antifungal properties as well as photocatalytic dye degradation efficiency.

Microbial resistance to conventional agents and the persistent contamination of water by synthetic dyes remain serious global challenges. Zinc Oxide nanoparticles (ZnO NPs) are well known for reactive oxygen species driven antibacterial action and photocatalytic dye degradation, yet they tend to aggregate and lose activity in aqueous environments. Biopolymers such as sodium alginate (SA) can provide a hydrophilic, biocompatible support, while CTAB can act as a cationic surfactant to disperse and stabilize ZnO. Only a few studies have attempted to integrate ZnO, CTAB and alginate into a single nanocomposite, and none has systametically examined how this synergy influences both antimicrobial and photocatalytic behaviour.

In this study we design and synthesise ZnO@CTAB-SA polymer nanocomposites via an *insitu* approach, evaluate their structural, antibacterial, antifungal, and dye-degradation properties, and discuss the mechansma that connect microstructure with performance. We hypothesise that combining ZnO with CTAB and alginate will (i) enhance dispersion and crystallinity, (ii) increase generation of reactive oxygen species for bacterial/fungal inhibition, and (iii) provide abundant adsorption sites for fficient photocatalytic removal of cationic and anionic dyes.

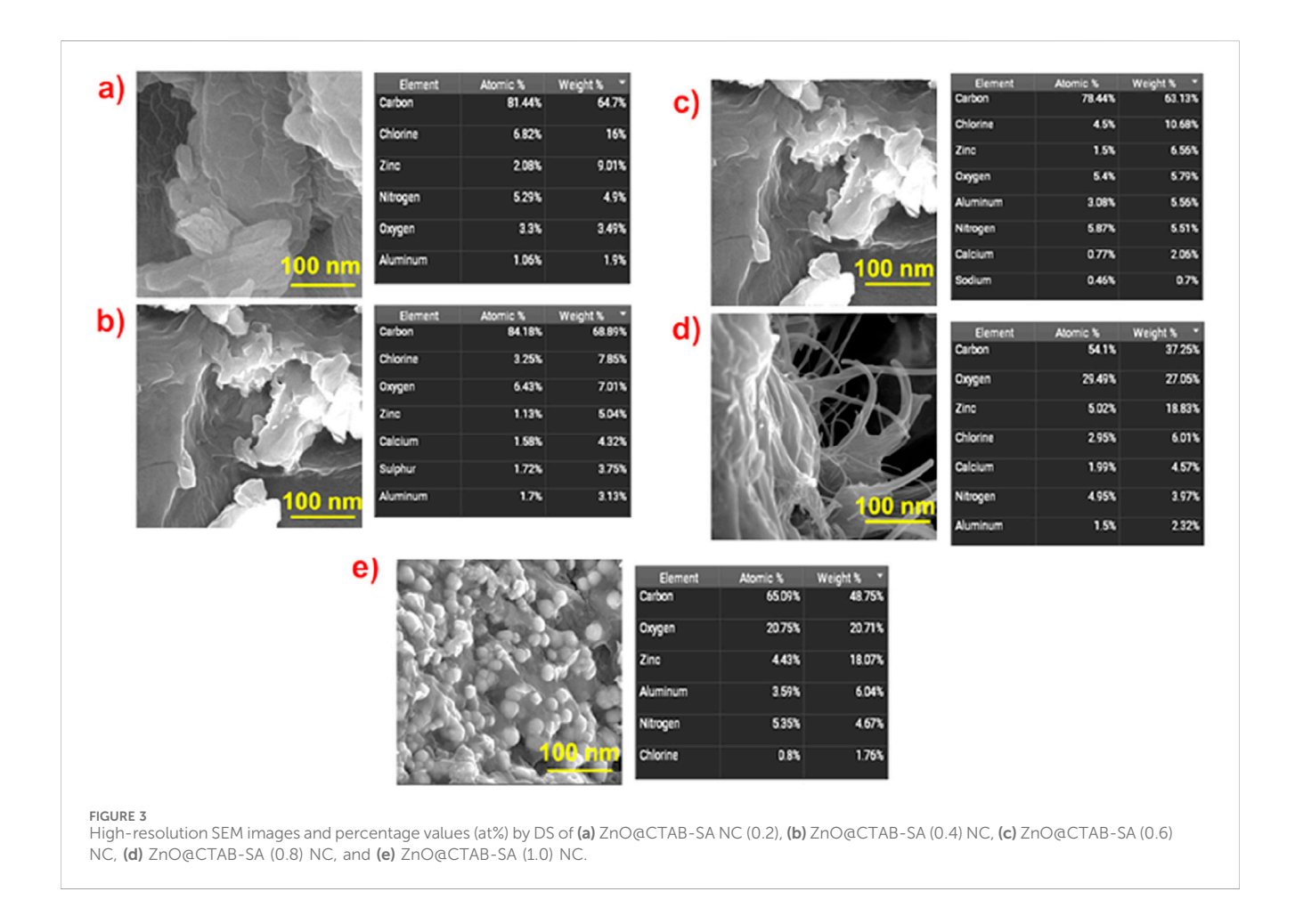
2 Experimental

2.1 Chemicals and reagents

All reagents and solvents were of analytical quality and were not subjected to additional purification prior to use. Zinc acetate dehydrate (99% purity), CTAB (99% purity), and sodium alginate polymers were acquired from SD Fine Chemicals. Sodium hydroxide pellets and ethanol (99% purity) were acquired from BLD Pharma. We acquired nutritious broth, agar-agar, Rhodamine B, and Alizarin Red S from SD Fine Chemicals.

2.2 Synthesis of zinc oxide NPs

Zinc oxide nanoparticles were produced via the sol-gel technique. Firstly, 2 g of zinc acetate dihydrate were dissolved in



15 mL of distilled water, and 8 g of sodium hydroxide were dissolved in 10 mL of distilled water. The solutions were agitated for roughly 5 minutes each. Sodium hydroxide solution was added to the zinc acetate solution after complete mixing, with continuous agitation using a magnetic stirrer for roughly 5 minutes. A burette was filled with 100 mL of ethanol and titrated dropwise into a solution of sodium hydroxide and zinc acetate. After the reaction, a white precipitate was formed, which was then washed three times with deionized water and ethanol, and subsequently dried at 120 °C in a hot air oven. The dried precursor was calcined at 900 °C for 2 hours to ensure complete removal of organics and formation of the wurtzite ZnO phase (JCPDS 36-1,451) (Mallakpour and Behranvand, 2016).

2.3 Synthesis of ZnO @CTAB-SA polymer nanocomposites

ZnO@CTAB-SA polymer nanocomposites were produced by an *in-situ* polymerization method. Initially, 0.7 mmol of ZnO nanoparticles were suspended in 50 mL of deionized water using ultrasonication for 30 min. Thereafter, an equimolar combination of CTAB and SA was dissolved in the ZnO suspension while maintaining continuous magnetic stirring. The solution was heated to 40 $^{\circ}$ C and subsequently permitted to cool gradually to ambient temperature. A series of nanocomposite samples with

differing ZnO nanoparticle concentrations Table 1 (10%, 20%, 30%, 40%, and 50%) were synthesized while preserving an equimolar ratio of CTAB and SA. The resultant mixture underwent centrifugation twice, was rinsed with alcohol and deionized water, and subsequently dried overnight in an oven at 60 °C (Mallakpour and Behranvand, 2016). Each synthesis batch yielded ~1.2–1.5 g of ZnO NPs, and a total of five batches were prepared under identical conditions to ensure reproducibility.

2.4 Biological studies of zinc nano composites

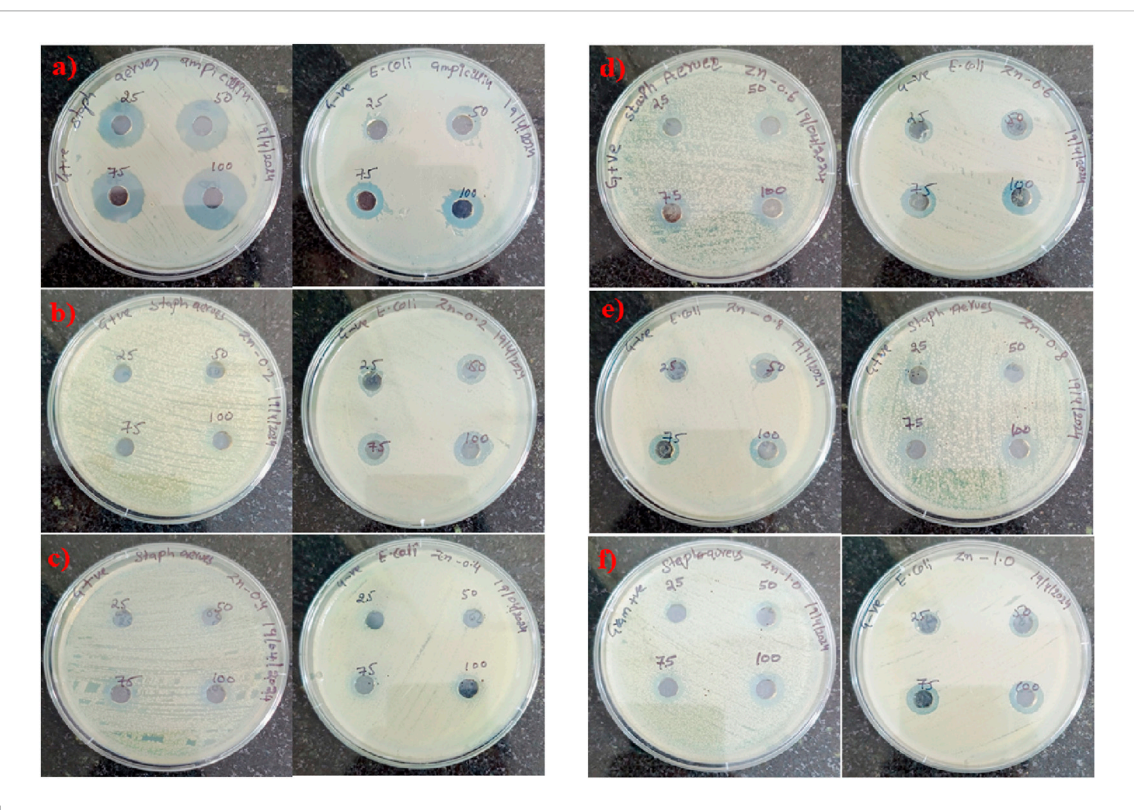
2.4.1 Anti-bacterial activity

2.4.1.1 Bacterial strains

The bacterial strains employed in this investigation, comprising the Gram-positive *Staphylococcus aureus* (ATCC 25923) and the Gram-negative *E. coli* (ATCC 25922), were obtained from ATCC.

2.4.1.2 Preparation of media for microbial activity

2.4.1.2.1 The medium of nutrient agar. Nutrient Agar was procured from a commercial vendor, and 28.0 g of the substance was accurately measured and dissolved in 1,000 cc of distilled water, ensuring thorough mixing. Autoclaved the dissolved nutrient agar at 121 °C for 15 min and employed the medium for plate preparation to assess its effect on microbial growth.



The effectiveness of ZnO@CTAB-SA composites (a) Positive Control, (b) 0.2, (c) 0.4, (d) 0.6, (e) 0.8) and (f) 1.0 against Gram + ve S aureus and Gram -ve E. coli was evaluated at different concentrations (25, 50, 75, and 100 100 µg/mL), in comparison with a standard agent.

TABLE 3 Depicts the Antibacterial activity of ZnO@CTAB-SA nanocomposites.

Strain/polymer nanocomposites	Anti-bacterial activity		Concentration (µg)/inhibition zone (mm)			nm)
S.No	Polymer nanocomposites	Strain	25	50	75	100
1	Standard Gram +ve	S. aureus	17	20	21	25
	Standard Gram -ve	E. coli	11	13	14	16
2	ZnO@CTAB-SA (0.2)	S. aureus	0	0	0	0
		E. coli	7	9	12	15
3	ZnO@CTAB-SA (0.4)	S. aureus	0	0	9	10
		E. coli	0	0	9	9
4	ZnO@CTAB-SA (0.6)	S. aureus	0	0	11	9
		E. coli	0	0	0	9
5	ZnO@CTAB-SA (0.8)	S. aureus	0	7	9	12
		E. coli	7	11	12	14
6	ZnO@CTAB-SA (1.0)	S. aureus	0	13	14	16
		E. coli	11	12	14	15

2.4.1.2.2 Broth with nutrients. Nutrient Broth was obtained from an official provider, with 1.3 g of the powder dispersed in 100 mL of distilled water and mixed thoroughly. The broth containing nutrients had been sterilized in an autoclave at 121 °C for 15 min and thereafter utilized for inoculum preparation.

2.4.1.2.3 Fabrication of standard solution. The initial culture of each organism was created using two nutrient agar slants and carefully sub-culturing each confirmed test organism. One slant set was maintained as a reference culture, but another was employed as an active culture. The bacterial cultures were preserved on suitable

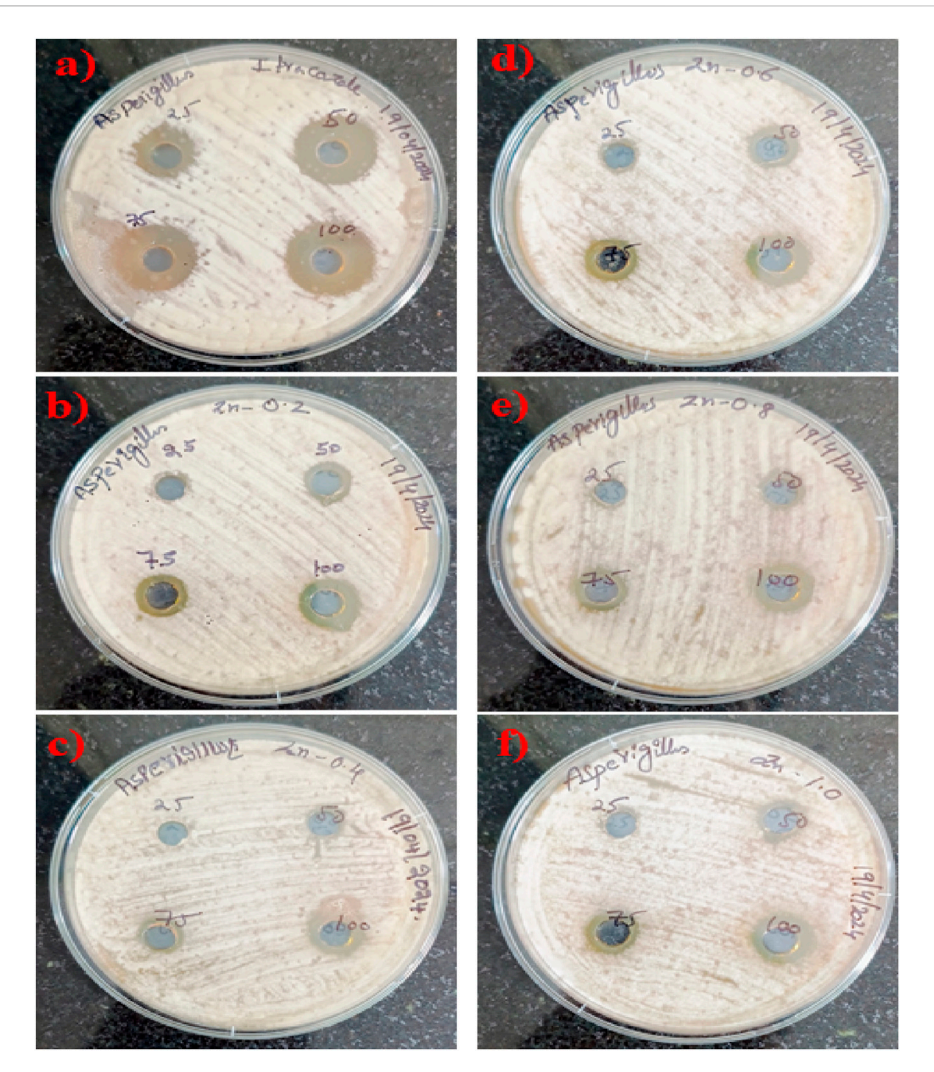


FIGURE 5
Zone of inhibition (mm) exhibiting the effectiveness of ZnO@CTAB-SAnano composites (a) Positive Control, (b) 0.2, (c) 0.4, (d) 0.6, (e) 0.8 and (f) 1.0 and the standard agent against Aspergillus niger at various concentrations (25, 50, 75, and 100 µg). The standard demonstrates a dose-dependent enhancement in effectiveness, whereas ZnO@CTAB-SA composites display moderate efficacy against fungal strains, with ZnO@CTAB-SA (1.0) achieving the highest performance among the evaluated nanocomposites.

surfaces of agar at 4 $^{\circ}$ C and utilized as stock cultures. One glycerol standard solution was also preserved at an ambient temperature of 20 $^{\circ}$ C.

2.4.1.2.4 The culture formulation. The chosen pathogens of bacteria were introduced into nutrient broth and incubated at 37 $^{\circ}$ C for 24 h. The resulting suspensions were verified to yield around 10–5 CFU/mL.

2.4.2 Inhibition of fungi

2.4.2.1 Fungal strains

The Aspergillus niger (MTCC 183) fungal strain utilized in this study was sourced from the Microbial Type Culture Collection (MTCC) at the Institute of Microbial Technology (IMTECH) in Chandigarh.

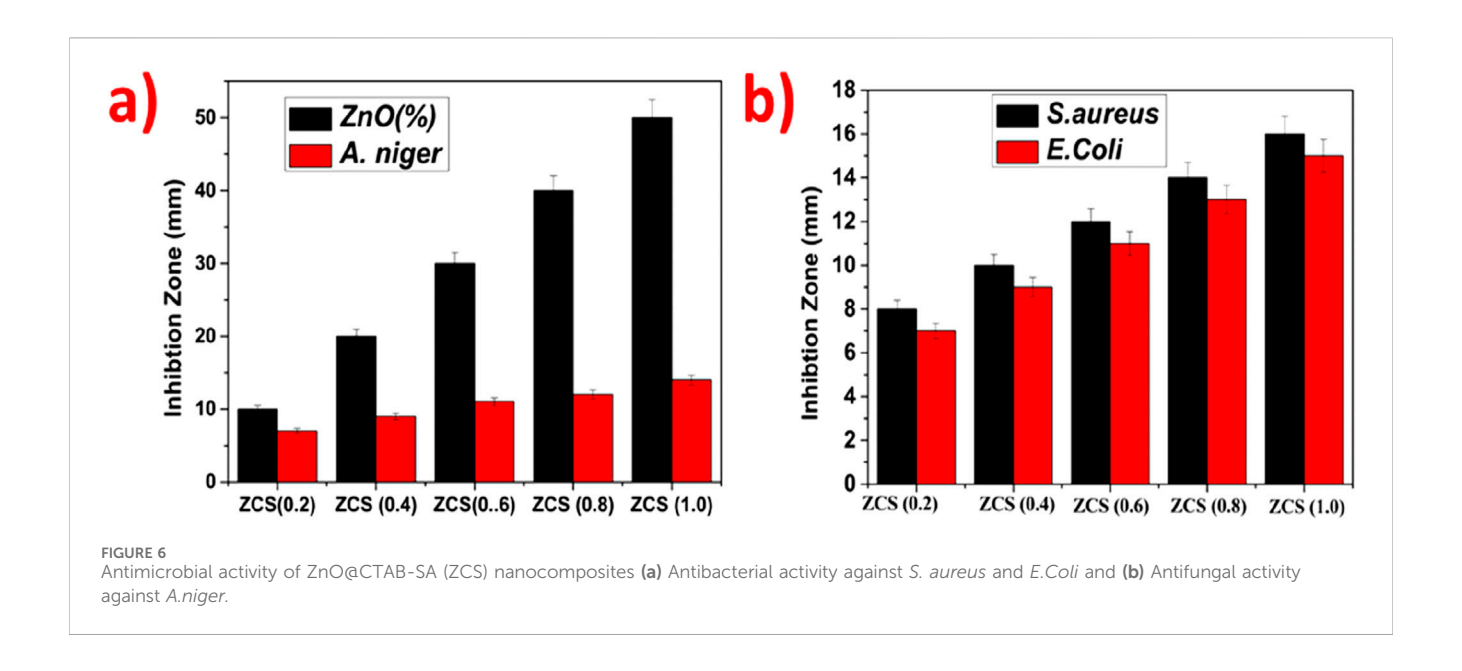
2.4.2.2 Sabouraud dextrose agar (SDA)

Sabouraud dextrose agar was commercially obtained and prepared by dissolving 32.5 g of the powder in 500 cc of distilled

water. To examine the effects on fungal organisms, the dissolved SDA was sterilized in an autoclave set at 121 °C for 15 min. The SDA was then used to prepare plates.

2.5 Dye adsorption degradation study

The photocatalytic characteristics of the synthesized ZnO@ CTAB-SA polymer nanocomposites were assessed utilizing Rhodamine B dye and Alizarin Red S. The degradation of Rhodamine B dye was analyzed with the catalyst (ZnO@CTAB-SA) under solar irradiation. Rhodamine B dye is an organic dye commonly employed in the textile industry for coloring purposes. It exhibits a distinctive absorbance band in the visible spectrum at 553 nm, as observed in UV-visible spectroscopy, while Alizarin Red S shows an absorbance band in the visible spectrum at 365 nm in UV-visible spectroscopy. In this study, 20 mg of synthesized nanoparticles were dispersed in 20 mL of double-distilled water



and sonicated for 5 min. The resulting sample solution was then added to 20 mL of Rhodamine B solution (2 × 10-5M) and 20 mL of Alizarin Red S in a separate conical flask. The mixed solutions were stirred for a few minutes and sonicated for half an hour in a darkroom. An adsorption-desorption equilibrium was established between the nanoparticles and the dyes without solar irradiation. The mixed reaction solution was then exposed to solar light. The experiment took place on a sunny day from 10 a.m. to 5 p.m., with an atmospheric temperature of 31 °C-38 °C. The mixed reaction solution was kept under solar irradiation with constant stirring. A 2 mL aliquot of the reaction mixture was taken at designated time intervals and filtered to remove the solid phase. The resulting filtrate was analyzed by recording the absorbance at 553 nm and 365 nm using a UV-Visible spectrophotometer. The absorbance of the Rhodamine B dye decreased at 553 nm (λ max) as the reaction time increased. Likewise, the absorbance of the Alizarin Red S dye decreased at 365 nm (\lambda max) with increasing reaction time. The findings demonstrated that Rhodamine B and Alizarin Red S were decolorized and degraded into new intermediate products. The percentage of degradation dyes was calculated using the following equation,

% of Degradation =
$$100*[(A_o - A_t)/A_o]$$

Here, A_o = Initial absorption of dye
 A_t = Absorbance of dye at the time, t

2.6 Photocatalytic degradation kinetic study of dyes

The kinetic study of photocatalytic degradation of dyes was evaluated by using synthesized Zn@CTAB-SA (1.0) under solar light irradiation. The Langmuir–Hinshelwood kinetic model provides an explanation for the photocatalytic degradation of organic dyes through the use of a heterogeneous photocatalyst, with duplicate

replications conducted and average results utilized for calculations. The following equation can apply for the photocatalytic reaction of dyes,

$$Rate(r) = dC/dt = k KC/1 + KC$$

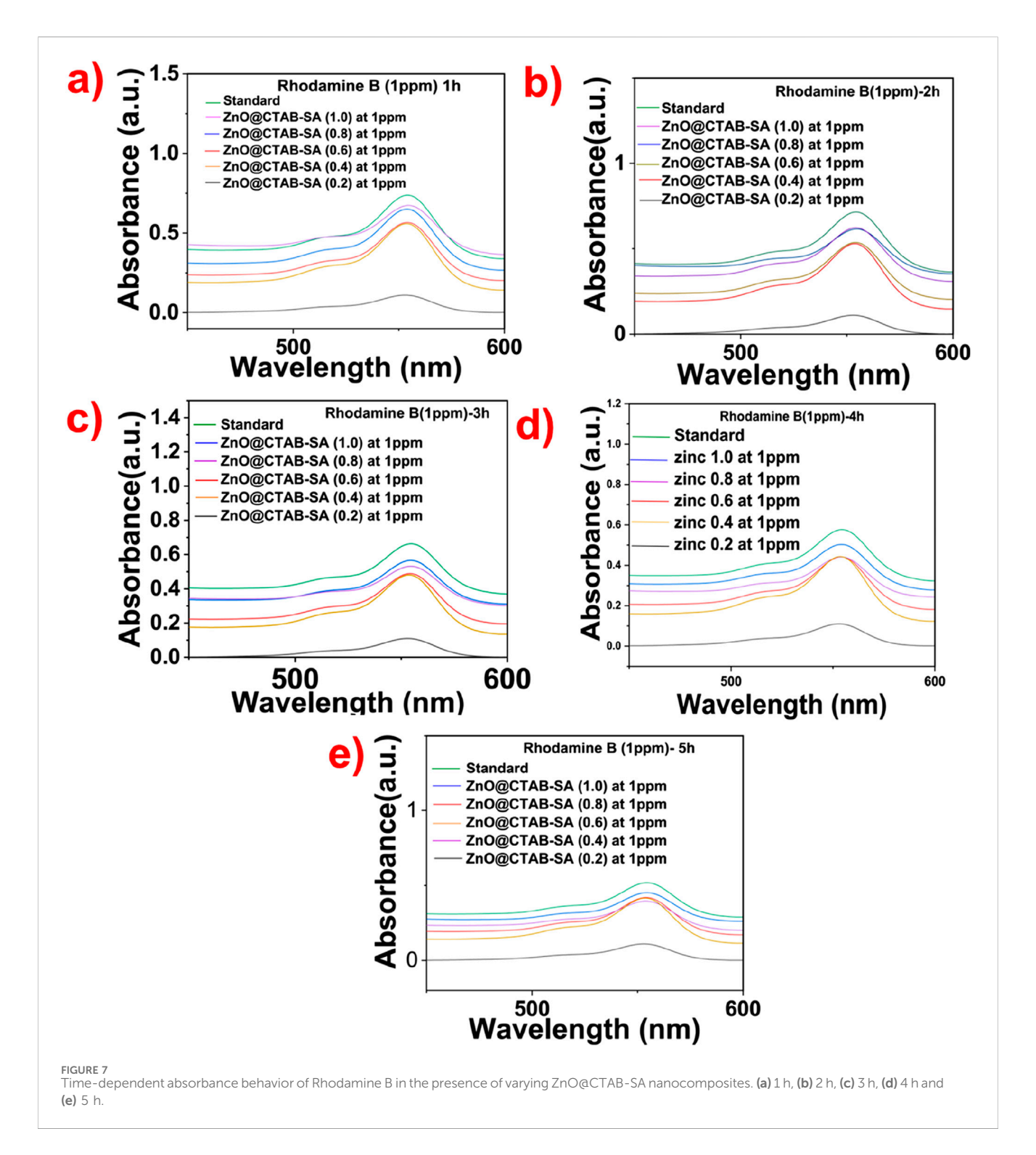
However, for the low concentration of dyes, KC<<1 and then followed by integrating concerning time t, the resultant equation is ln $(C_o/C_t) = k$ Kt = k_{app} t. It is a pseudo-first-order kinetic model equation.

Then the equation is modified as $\ln (A_o/A_t) = K_{app} t$.

Here, dC/dt = rate of dye degradation (mg/L.min⁻¹), k = the reaction rate constant (min-1), K = the absorption coefficient of the dye on to the photocatalyst, Kapp (min-1) is the apparent rate constant.

2.7 Characterization

A wide variety of analytical methods were employed to characterize the substance. An Agilent ATR benchtop spectrometer 4,500-400 cm⁻¹ using a KBr spectrometer was used to obtain the FT-IR spectra, which were recorded in the 400-4,000 cm⁻¹ range. The Rigaku Ultima IV powder diffractometer, operated at 40 kV with a CuKa radiation source, was used to analyse structural phase parameters using X-ray diffraction (XRD) in the 2θ range of 10°-80°. A scanning electron microscope (ZEIS Evo SEM, EDS Oxford instruments) was used to analyse the morphology and particle size. The particle size of the ZnO and ZnO@CTAB-SA nanocomposites was measured from SEM images taken at a scale of 100 nm. A total of 70 particles were randomly selected from the micrographs for size measurement. The particle diameters were measured using ImageJ software, and the average size, along with the standard deviation, was calculated to provide a representative size distribution.



3 Results and discussion

3.1 Structural and morphological analysis

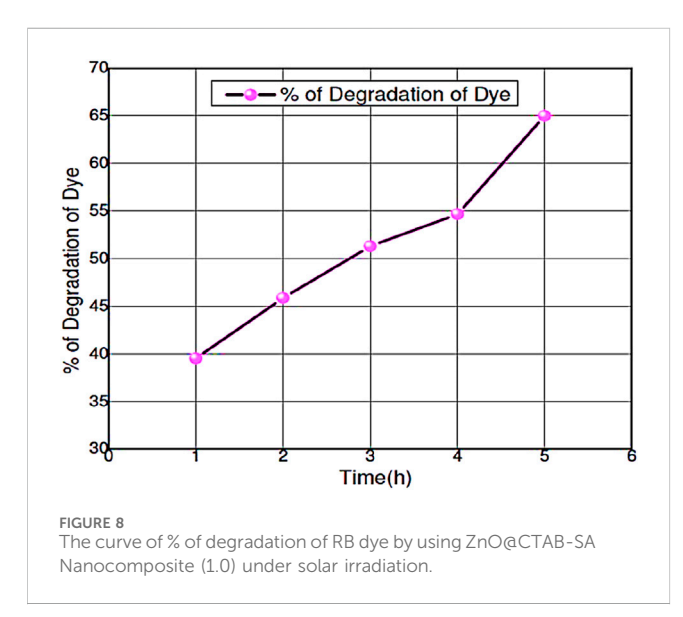
3.1.1 FTIR analysis

In Figure 1 shows the infrared (IR)Spectrum of Zinc Composites (SA and CTAB polymers at different concentrations) along with pure ZnO for comparison. The broad peak was observed at 3,400 cm⁻¹, indicating the O-H stretching vibrations in sodium

alginate polymer and ZnO NPs (Motelica et al., 2021). Some well-defined peaks seen at 2,915 cm⁻¹ and 2,844 cm⁻¹ indicate the C-H stretching vibrations in alkyl chains of CTAB on the surface of ZnO NPs, the peaks at 1,633 cm⁻¹ and 1,600 cm⁻¹ (C=O) suggest the interaction between Carboxylate groups (SA) and ZnO NPs. The peaks at 1,401 cm⁻¹ (C-H) bending vibration further support the presence of CTAB and SA, and 1,122 cm⁻¹ (C-O-C) stretching vibration in SA. In addition, the peaks at 673 cm⁻¹ and 621 cm⁻¹ correspond to the stretching vibrations of ZnO bonds, providing

TABLE 4 Depicts the Antifungal activity of Zn@SA-CTAB nonocomposites.

Strain/polymer nanocomposites	Anti-fungal activity	Concentration (µg)/zone of inhibition (mm		oition (mm)	
S No	Strain/Polymer nanocomposite	25	50	75	100
1	Aspergillus niger	11	17	18	20
2	ZnO@CTAB-SA (0.2)	0	12	13	14
3	ZnO@CTAB-SA (0.4)	0	9	10	13
4	ZnO@CTAB-SA (0.6)	0	9	12	14
5	ZnO@CTAB-SA (0.8)	0	11	12	14
6	ZnO@CTAB-SA (1.0)	9	11	12	14



evidence of the existence of ZnO nanoparticles (Motelica et al., 2021; Salama et al., 2018). The bands at 673 and 621 cm⁻¹ were initially assigned to Zn-O stretching. While bulk ZnO usually shows transverse-optical modes near 430–560 cm⁻¹ (E₁ (TO), A₁ (TO)), several studies have reported a shift toward higher wavenumbers when ZnO is present as nanosized particles or is strongly bound to polymers/surfactants (Djurišić and Leung, 2006; Loste et al., 2019). Interaction of Zn²⁺ with the carboxylate groups of sodium alginate and with CTAB micelles may stiffen the Zn-O bond, producing a blue shift of the stretching band. Similar upshifts (610–680 cm⁻¹) were observed for ZnO encapsulated in biopolymers. Therefore, the higher frequency in our spectrum is consistent with nanosized ZnO coordinated to the SA/CTAB matrix rather than bulk ZnO.

3.1.2 PXRD analysis

The PXRD pattern of the synthesized ZnO@CTAB-SA nanocomposites (Figure 2) exhibits characteristic diffraction peaks at 22.3°, 26.6°, 30.76°, and higher intensity peaks at 32.59°, 38.29°, 44.27°, 46°, and 50.26° on these peaks 32.59°, 38.29°, 44.27°, 46°, and 50.26°, which can be indexed to the (100), (002), (101), (102), and (110) planes these are stimulated with (JCPDS card no.

TABLE 5 The values of % of degradation of RB dye by using Zn@CTAB-SA (1.0) nanocomposites under solar irradiation.

Time (h)	Abs	% Of degradation of dye
0	0.805	0.00
1	0.487	39.50
2	0.436	45.84
3	0.392	51.30
4	0.365	54.66
5	0.282	64.97

36-1,451) (Supramaniam et al., 2021). A comparison of standard and observed diffraction data is summarized in Table 2. Minor peak shifts and a decrease in relative intensity were observed in the composites, which may be attributed to lattice strain and the interaction between ZnO nanoparticles and the sodium alginate-CTAB polymer matrix. Additional peaks at lower angles (22.3°, 26.6°, 30.76°) are attributed to the polymeric components (Sodium alginate and CTAB) and possible amorphous organic residues. Similar features have been reported in polymer-based nanocomposites containing ZnO NPs (Li et al., 2018). Significant variations in peak intensities, such as the notably strong peak near 47° observed in ZnO@CTAB-SA (0.6) compared to the prevalent intensity near 44° in other samples, are attributed to differences in nanoparticle size distribution, morphology, and preferential orientation within the polymer matrix. These peaks do not correspond to ZnO or any impurity phases. The slight shifts and intensity variations of ZnO peaks are due to strain and strong interfacial interactions in the composite, typical of such systems. No other crystalline phases were detected, confirming the retained purity of the ZnO wurtzite structure in the composites.

3.1.3 FESEM analysis

In Figure 3, we observed the FE SEM images of Zinc polymer nanocomposites (0.2), (0.4), (0.6), (0.8), and (1.0) indicating that the shape and structure vary with increasing zinc content. Zinc composites 0.2 exhibit smooth, thin, sheet-like structures characterized by a medium level of porosity. Conversely, zinc composites 0.4 exhibit a greater presence of interconnected and

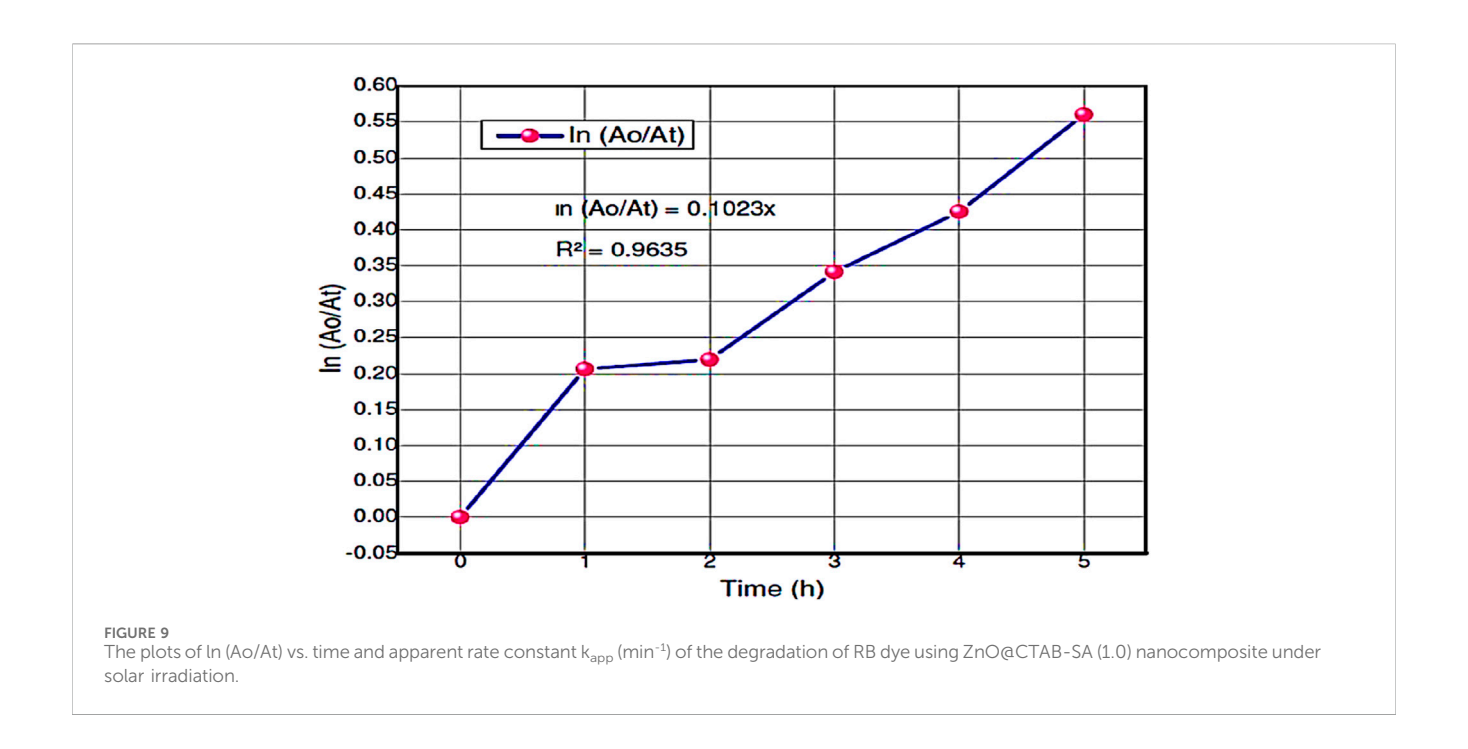


TABLE 6 The values of Ao/At and In (Ao/At) of RB dye using ZnO@CTAB-SA (1.0) nanocomposite under solar irradiation.

Time (h)	Ao/At	ln (Ao/At)	
0	0.0000	0.0000	
1	1.6084	0.2064	
2	1.6584	0.2197	
3	2.1945	0.3413	
4	2.6611	0.4251	
5	3.6327	0.5602	
RB dye	Apparent rate constant, Kapp (min ⁻¹) = 0.1023	$R^2 = 0.9635$	

aggregated flakes, resulting in a highly porous structure. With an increase in Zinc concentration levels, the zinc composites at concentrations of 0.6, 0.8, and 1.0 exhibit greater particle agglomeration, resulting in denser and more compact structures. The EDS analysis indicates that this alteration in shape corresponds with the modifications in the composition of the materials. The composites consist of a carbon-rich matrix containing varying quantities of zinc, chlorine, and oxygen, indicating that the surfaces have undergone modification and doping with an increase in porosity and the functionalization involving zinc and other elements. There is a corresponding rise in both surface area and the availability of active sites.

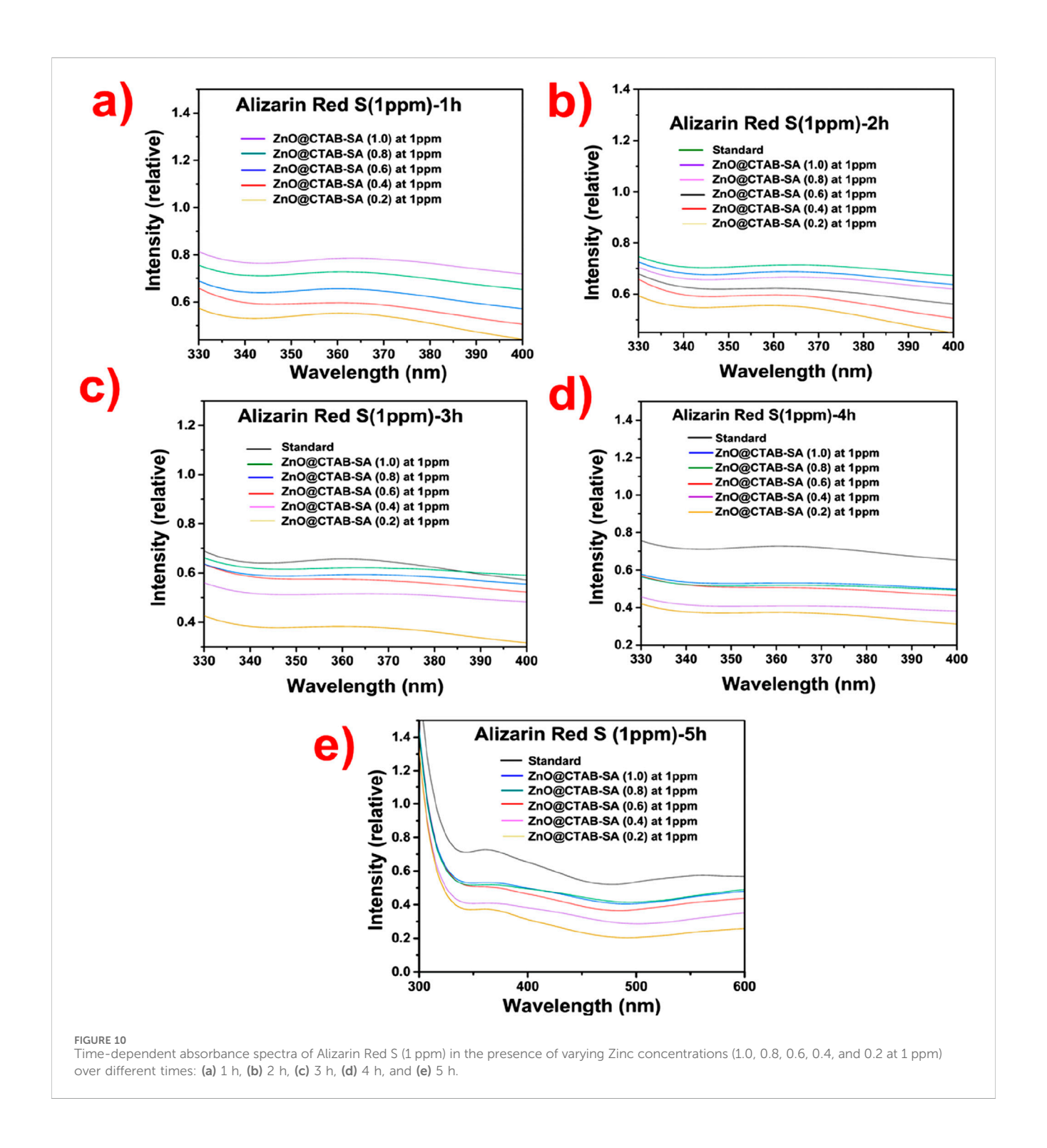
3.2 Antibacterial activity

Zinc, recognized as a highly effective antimicrobial agent, is particularly useful in its nanoparticle or oxide forms, which facilitate the generation of reactive oxygen species (ROS).

Salicylic Acid, categorized as a phenolic compound, demonstrates mild antibacterial activity along with a robust chelating ability, which enhances the release of Zn ions and boosts surface reactivity. CTAB, a cationic surfactant, plays a role in disrupting the membranes of bacteria (Figure 4).

The efficacy of compounds was assessed via the Agar well-diffusion method at four distinct concentrations (25, 50, 75, and 100 $\,\mu L)$ against multiple bacterial pathogens, including Staphylococcus aureus and E. coli (Varun Kumar and Reddy, 2023). The plates were incubated at 37 °C for 18–24 h, after which the diameter of the inhibitory zone (mm) was measured, and the activity index was calculated. The measurements were performed in four specific fixed orientations, and the average values were shown in Table 3.

The antibacterial efficacy of ZnO@CTAB-SA composites was evaluated against *Staphylococcus aureus* (Gram-positive) and *E. coli* (Gram-negative), and compared with a standard antibacterial agent observed in Table 1. Figures 5a, 7 a illustrates that the standard exhibited strong and consistent antibacterial activity, with inhibition zones ranging from 17 to 25 nm for *S. aureus* and 11–16 mm for



E. coli. Among the composites, ZnO@CTAB-SA (0.2) exhibited minimal activity against S. aureus while demonstrating modest activity against E. coli, reaching a maximal inhibition zone of 15 mm at a concentration of 100 μg/mL (Figure 5b). ZnO@CTAB-SA (0.4) and ZnO@CTAB-SA (0.6) demonstrated concentrations, resulting in inhibition zones of 10 mm and 11 mm for S. aureus respectively (Figures 5c,d). ZnO@CTAB-SA (0.8) demonstrated enhanced effectiveness against both bacterial strains, achieving inhibition zones of 12 mm for S. aureus and 14 mm for E. coli at a concentration of 100 μg/mL (Figure 5e). ZnO@

CTAB-SA (1.0) exhibited the highest antibacterial activity among the composites, showing inhibition zones of 16 mm for *S. aureus* and 15 mm for *E. coli* at a concentration of 100 µg/mL (Figure 5e), which is comparable to the standard this may be due to the higher zinc concentration in the composites enhances the reactive oxygen species, damaging bacterial membranes and intracellular components and its increases zinc ions reduce bacterial enzymatic activity and growth and it's functionalizing the surface of the composite increases its binding affinity to bacterial cell walls, especially Gram-positive *S. aureus* having thick peptidoglycan



TABLE 7 The values of % of degradation of Alizarin Red S dye by using ZnO@CTAB-SA (1.0) nanocomposites under solar irradiation.

Time (h)	Abs	% Of degradation of dye
0	0.801	0.00
1	0.573	28.46
2	0.519	35.21
3	0.407	49.19
4	0.384	52.06
5	0.329	58.93

% of degradation of dye = (100- (Abs at 1, 2, 3, 4- and 5-h x 100)/Abs at 0 h). Example at 1 h = (100-(0.573 \times 100)/0.801) = 28.46%.

barrier. This composite is the most efficient antibacterial composite and microbial control.

3.3 Antifungal activity

The efficacy of drugs against fungal proliferation was assessed utilizing the Agar well diffusion technique, incorporating four distinct doses of the test compound (25, 50, 75, and 100 μL). The prepared SDA culture plates were infected with Aspergillus niger using the spread plate technique (Sujith Benarzee et al., 2023). The plates were maintained at a temperature of 37 °C \pm 2 °C for 48 h to evaluate fungal growth. Following a 48-h incubation period, the plates were assessed for the existence of zones surrounding the wells, and the dimensions of the inhibition zones (mm) were recorded, alongside the computation of the activity index. The measurements were performed in three specific fixed orientations throughout all three replicates, and the average values were summarized in Table 4.

The antifungal efficacy of ZnO@CTAB-SA composites at varying concentrations (0.2, 0.4, 0.6, 0.8, and 1.0) was assessed

against Aspergillus niger and compared with a standard antifungal drug (Figures 6a, 7b). The results showed a notable dose-dependent antifungal effect, with inhibition zones ranging from 11 mm at 25 µg to 20 mm at 100 µg. Among the composites, ZnO@CTAB-SA (0.2) (Figure 6b) demonstrated slight activity, with inhibitory zones starting at 12 mm at 50 µg and rising to 14 mm at 100 µg. ZnO@CTAB-SA (0.4) and (0.6) (Figure 6) displayed similar patterns, with maximum inhibition zones of 13 mm and 14 mm, respectively, at a concentration of 100 µg. ZnO@CTAB-SA (0.8) (Figure 6) demonstrated slightly improved activity, showing inhibition zones of 11 mm, and 14 mm at a concentration of 50,100 μg. ZnO@CTAB-SA (1.0) (Figure 6) exhibits exceptional performance among the composites, exhibiting a 9 mm, and 14 mm, inhibitory zone at the minimum concentration of 25 µg, which expanded to 14 mm at 100 µg. Although all composites demonstrated significant antifungal activity, none surpassed the effectiveness of the standard, indicating a potential for future enhancement of the ZnO@CTAB-SA composite formulation.

3.4 Dye adsorption and photocatalytic degradation study

The ZnO@CTAB-SA nanocomposites were evaluated for the removal of Rhodamine B (cationic dye) and Alizarin Red S (anionic dye), both of which are widely used in textiles, food coloring, printing, and biological staining. Initially, all dye solutions containing the composites were kept in the dark for 30 min to establish adsorption-desorption equilibrium. This step confirmed the adsorption capacity of the nanocomposites. Upon subsequent exposure to UV-visible light for 1–5 h, a significant decrease in absorbance intensity was observed, confirming photocatalytic degradation. Among the samples, ZnO@CTAB-SA (1.0) exhibited the highest degradation efficiency, attributed to the synergistic effect of adsorption by the polymer matrix and photocatalysis by ZnO NPs (Chinthamreddy et al., 2024).

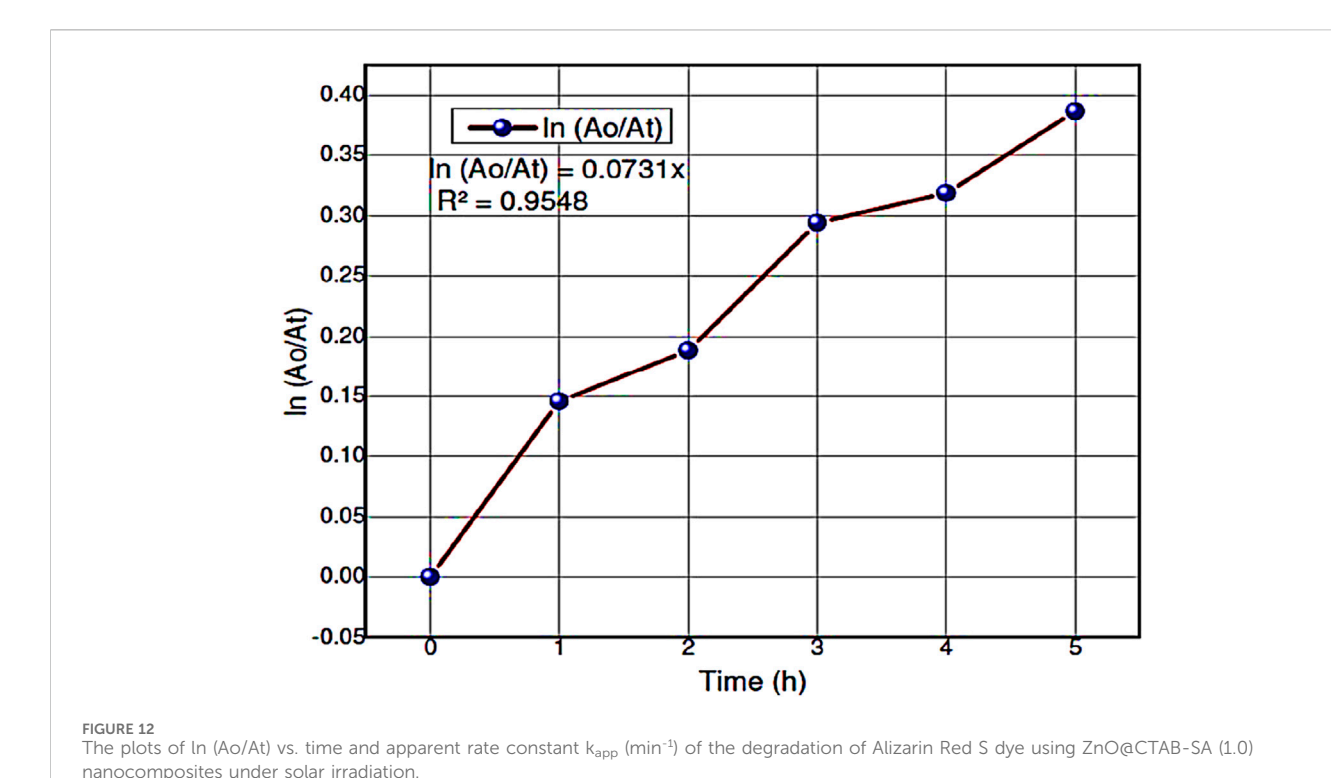


TABLE 8 The values of Ao/At and In (Ao/At) of Alizarin Red S dye using ZnO@CTAB-SA (1.0) nanocomposites under solar irradiation.

Time (h)	Ao/At	ln (Ao/At)
0	0.000	0.0000
1	1.399	0.1457
2	1.543	0.1884
3	1.969	0.2942
4	2.084	0.3188
5	2.436	0.3867
Alizarin red S dye	Apparent rate constant, Kapp $(min^{-1}) = 0.0731$	$R^2 = 0.9548$

3.4.1 Rhodamine B dye adsorption

Figure 8, we observed the analysis of Rhodamine B degradation, which involved observing its distinct absorbance peak at ~ 553 nm throughout 1–5 h using ZnO@CTAB-SA nanocomposites. The findings demonstrate a gradual decrease in absorbance as the concentration of ZnO@CTAB-SA rises (0.2,0.4,0.6,0.8, and 1.0). At ZnO@CTAB-SA (0.2), there is a noticeable reduction in photocatalytic activity, attributed to the limited active sites for dye interaction. With the rise in the concentration of ZnO@CTAB-SA (0.2 and 0.4), there is a noticeable enhancement in photocatalytic efficiency, demonstrated by a steady reduction in absorbance intensity. The most notable decline is observed at ZnO@CTAB-SA (0.8) and (1.0) composites, where there is a marked reduction in the absorbance peak, especially following the 5-h treatment. The improved degradation is linked to the effective

production of reactive oxygen and electrostatic interactions between the positively charged Rhodamine B dye and the ZnO@ CTAB-SA nanocomposites.

3.4.2 Percentage of degradation of RB dye using ZnO@CTAB-SA (1.0)

The percentage of degradation of the RB efficacy in the presence of ZnO@CTAB-SA (1.0) nano composites was evaluated under solar irradiation, and results are shown in Figure 8. The mathematical equation, % Degradation = 100* [(A_o-A_t)/A_o], was used to calculated % of degradation of RB dye during the reaction, where A_o and A_t are the absorbance of RB dye (λ_{max} = 553) at the initial and the time, t. Table 5 shows the calculated % of degradation of RB dye using synthesized ZnO@CTAB-SA (1.0) under solar irradiations.

% of Degradation of dye = (100- (Abs at 1, 2, 3, 4 and 5 h x 100)/ Abs at 0 h)

Example at 1 h= $(100-(0.487 \times 100)/0.805) = 39.50\%$

3.4.3 Photodegradation kinetics of RB dye

The Langmuir–Hinshelwood (L-H) equation can explain the reactivity results and gives the reaction rate values for the degradation of hours during photocatalysis reaction. The reaction rate constant (k)and correlating factor value were calculated for RB dye during the degradation by plotting $\ln (A_o/A_t)$ versus irradiation time. Figure 9 shows the reaction rate constant and correlating factor value of this experiment. This photocatalytic degradation of RB dye follows pseudo-first-order kinetic reaction. The $\ln (A_o/A_t)$ was calculated based on the absorbance of RB dye during the catalytic reaction. The resultant values are shown in Table 6.

3.4.4 Alizarin Red S dye adsorption

The photocatalytic degradation of Alizarin Red S (Figure 10), an anionic dye, by observing its absorbance peak at ~ 365 nm while utilizing ZnO@CTAB-SA nanocomposites over a duration of 1–5 h. At the minimal ZnO@CTAB-SA (0.2), there is merely a slight reduction in absorbance, suggesting limited degradation of the dye. The ZnO@CTAB-SA (0.4), and (0.6), there is a clear enhancement in photocatalytic activity, accompanied by additional decreases in absorbance. Significant degradation of Alizarin Red S occurs at elevated concentrations of ZnO@CTAB-SA (0.8), and (1.0), especially after a duration of 4–5 h.

The ZnO@CTAB-SA nanocomposites show significant effectiveness in degrading Rhodamine B (a cationic dye) and Alizarin Red S (an anionic dye), improving photocatalytic efficiency as ZnO@CTAB-SA concentrations increase and exposure times extend. The interaction between the positively charged dye and the ZnO@CTAB-SA nanocomposites enhances the effectiveness of adsorption and leads to effective degradation. In contrast, the anionic nature of Alizarin Red S facilitates strong interactions with the positively charged ZnO@CTAB-SA nanocomposite surface, thereby improving degradation efficiency. Both dyes demonstrate notable decreases in absorbance, with Rhodamine B showing a marginally quicker degradation, probably attributed to more robust electrostatic interactions. The combined influence of the sodium alginate -CTAB matrix significantly boosts photocatalytic performance and achieves a consistent distribution of ZnO@CTAB-SA nanocomposites, rendering these nanocomposites exceptionally effective in eliminating both cationic and anionic dyes from water solutions.

3.4.5 Percentage of degradation of Alizarin Red S dye using ZnO@CTAB-SA (1.0)

The percentage of degradation of the Alizarin Red S efficacy in the presence of ZnO@CTAB-SA (1.0) nanocomposites was evaluated under solar irradiation, and results are shown in Figure 11. The mathematical equation, % Degradation = 100^{\ast} [(A_o-A_t)/A_o], was used to calculated % of degradation of Alizarin Red S dye during the reaction, where A_o and A_t are the absorbance of Alizarin Red S dye (λ_{max} = 365) at the initial and the time, t. Table 7 shows the calculated % of degradation of Alizarin Red S dye using synthesized Zn@CTAB-SA (1.0) under solar irradiations.

3.4.6 Photodegradation kinetics of Alizarin Red S dye

The Langmuir–Hinshelwood (L-H) equation can explain the reactivity results and gives the reaction rate values for the degradation of hours during photocatalysis reaction. The reaction rate constant (k)and correlating factor value were calculated for Alizarin Red S dye during the degradation plotting $\ln (A_o/A_t)$ versus irradiation time. Figure 12 shows the reaction rate constant and correlating factor value of this experiment. This photocatalytic degradation of Alizarin Red S dye follows pseudo-first-order kinetic reaction. The $\ln (A_o/A_t)$ was calculated based on the absorbance of Alizarin Red S dye during the catalytic reaction. The resultant values are shown in Table 8.

4 Conclusion

The synthesised ZnO@CTAB-SA polymer nanocomposites were efficient against Staphylococcus aureus, Escherichia coli, and Aspergillus niger. Sodium alginate, CTAB, and ZnO nanoparticles synergistically improved the composites structural characteristics and microbial cell contact, resulting in bioactivity. Additionally, the nanocomposites photocatalytically degraded industrial dyes Rhodamine B and Alizarin Red S, demonstrating their wastewater treatment potential. These findings indicate that ZnO@CTAB-SA composites could address microbial resistance and dye pollution. The ZnO@CTAB-SA polymer nanocomposites were effective against Staphylococcus aureus, E. coli, and Aspergillus niger. Sodium alginate, CTAB, and ZnO nanoparticles synergistically increased composite structure and microbial cell contact, resulting in bioactivity. The nanocomposites also degraded commercial dyes including Rhodamine B and Alizarin Red S photocatalytically, suggesting wastewater treatment potential. The results suggest that ZnO@CTAB-SA composites might confront microbiological resistance and environmental dye pollution. Synthesis and integration of these materials into biomedical and environmental systems are needed.

Data availability statement

The original contributions presented in the study are included in the article/supplementary material, further inquiries can be directed to the corresponding authors.

Author contributions

UP: Conceptualization, Formal Analysis, Writing – original draft. TR: Investigation, Writing – review and editing. YP: Writing – original draft, Investigation, Validation, Visualization. PG: Data curation, Funding acquisition, Project administration, Supervision, Writing – review and editing.

Funding

The author(s) declare that financial support was received for the research and/or publication of this article. Open access funding provided by corresponding author Institute (Jožef Stefan Institute, Jamova 39, SI-1000 Ljubljana, Slovenia).

Acknowledgments

The authors are thankful to Mahatma Gandhi University, Nalgonda, Telangana, India, for its research facility and continuous support.

Conflict of interest

Author TR was employed by Isosphere Biosciences Pvt Ltd.

The remaining authors declare that the research was conducted in the absence of any commercial or financial relationships that could be construed as a potential conflict of interest.

Generative Al statement

The author(s) declare that no Generative AI was used in the creation of this manuscript.

Any alternative text (alt text) provided alongside figures in this article has been generated by Frontiers with the support of artificial

intelligence and reasonable efforts have been made to ensure accuracy, including review by the authors wherever possible. If you identify any issues, please contact us.

Publisher's note

All claims expressed in this article are solely those of the authors and do not necessarily represent those of their affiliated organizations, or those of the publisher, the editors and the reviewers. Any product that may be evaluated in this article, or claim that may be made by its manufacturer, is not guaranteed or endorsed by the publisher.

References

Ambalgi, S. M., Inamdar, H. K., Manjula, V. T., Nagaraja, S., and Shrishail, G. (2016). Synthesis, characterization and electrical properties of polyaniline/nickel oxide nanocomposites. *Int. J. Eng. Res.* 5 (2), 119–122. doi:10.17950/ijer/v5s2/210

Ashhari, S., Sehhat, E., and Ranjbar, Z. (2023). Nanomaterial-based antibacterial and antiviral thin film coatings. ACS Symp. Ser. 1458, 203–250. doi:10.1021/bk-2023-1458. ch007

Bains, D., Singh, G., and Singh, N. (2022). Sustainable synthesis of ionic liquid-functionalized zinc oxide nanosheets (IL@ZnO): evaluation of antibacterial potential activity for biomedical applications. ACS Appl. Bio Mater. 5 (3), 1239–1251. doi:10.1021/acsabm.1c01258

Bao, Q., Zhang, D., and Qi, P. (2011). Synthesis and characterization of silver nanoparticle and graphene oxide nanosheet composites as a bactericidal agent for water disinfection. *J. Colloid Interface Sci.* 360 (2), 463–470. doi:10.1016/j.jcis.2011. 05.009

Canama, G. J. C., Delco, M. C. L., Talandron, R. A., and Tan, N. P. (2023). Synthesis of chitosan-silver nanocomposite and its evaluation as an antibacterial coating for Mobile phone glass protectors. *ACS Omega* 8 (20), 17699–17711. doi:10.1021/acsomega. 3c00191

Chinthamreddy, A., Koppula, S., Nallamalla, S. B., Karra, G., and Manabolu Surya, S. B. (2024). Synthesis and characterization of MOF polymer nanocomposites for chromium adsorption and their antimicrobial properties. *Chem. Phys. Impact* 8, 100599. doi:10.1016/j.chphi.2024.100599

Demirel, B., and Erol Taygun, M. (2023). Zinc oxide-doped antibacterial soda lime glass produced as a glass container. ACS Omega 8 (10), 9257–9264. doi:10.1021/acsomega.2c07469

Devi, N., Saima, N., Pandey, S. K., Kaur, D., Kumar, V., Sharma, R. K., et al. (2024). Membrane penetrating-cationic peptide BP100 functionalized silver nanoparticles as efficient antibacterial agents. ACS Appl. Nano Mater. 7 (5), 4731–4741. doi:10.1021/

Djurišić, A. B., and Leung, Y. H. (2006). Optical properties of ZnO nanostructures. Small 2 (8–9), 944–961. doi:10.1002/smll.200600134

El-Samak, A. A., Ponnamma, D., Hassan, M. K., Adham, S., Karim, A., Ammar, A., et al. (2021). Multifunctional oil absorption with macroporous polystyrene fibers incorporating silver-doped ZnO. *ACS Omega* 6 (12), 8081–8093. doi:10.1021/acsomega.0c05683

Garcia, M. M., Da Silva, B. L., Sorrechia, R., Pietro, R. C. L. R., and Chiavacci, L. A. (2022). Sustainable antibacterial activity of polyamide fabrics containing ZnO nanoparticles. *ACS Appl. Bio Mater.* 5 (8), 3667–3677. doi:10.1021/acsabm.

Gharpure, S., Yadwade, R., and Ankamwar, B. (2022). Non-antimicrobial and non-anticancer properties of ZnO nanoparticles biosynthesized using different plant parts of Bixa Orellana. ACS Omega 7 (2), 1914–1933. doi:10.1021/acsomega.1c05324

Hao, L., Zheng, Q., Guan, M., Zhou, M., Yin, Z., Chen, H., et al. (2023). Large ultrathin Polyoxomolybdate-Decorated boron nitride nanosheets with enhanced antibacterial activity for infection control. ACS Appl. Nano Mater. 6 (6), 4754–4769. doi:10.1021/acsanm.3c00247

Hosseini, M., Behzadinasab, S., Chin, A. W. H., Poon, L. L. M., and Ducker, W. A. (2021). Reduction of infectivity of SARS-CoV-2 by zinc oxide coatings. ACS Biomaterials Sci. Eng. 7 (11), 5022–5027. doi:10.1021/acsbiomaterials.1c01076

Izzi, M., Sportelli, M. C., Torsi, L., Picca, R. A., and Cioffi, N. (2023). Synthesis and antimicrobial applications of ZnO nanostructures: a review. ACS Appl. Nano Mater. 6 (13), 10881–10902. doi:10.1021/acsanm.3c01432

Kapoor, G., Saigal, S., and Elongavan, A. (2017). Action and resistance mechanisms of antibiotics: a guide for clinicians. *J. Anaesthesiol. Clin. Pharmacol.* 33 (3), 300–305. doi:10.4103/joacp.JOACP_349_15

Lee, K. Y., and Mooney, D. J. (2001). Hydrogels for tissue engineering. *Chem. Rev.* 101 (7), 1869–1880. doi:10.1021/cr000108x

Li, X., Zhang, J., Ju, Z., Li, Y., Xu, J., Xin, J., et al. (2018). Facile synthesis of Cellulose/ZnO aerogel with uniform and tunable nanoparticles based on ionic liquid and polyhydric alcohol. *ACS Sustain. Chem. Eng.* 6 (12), 16248–16254. doi:10.1021/acssuschemeng.8b03106

Loomba, P., Nallamalla, S. B., Mohan Reddy, A. J., Katari, N. K., and Manabolu Surya, S. B. (2025). Synthesis and characterization of high entropy MOFs as enhanced chemiresistive ammonia gas sensor agents. *J. Indian Chem. Soc.* 102 (4), 101631. doi:10.1016/j.jics.2025.101631

Loste, J., Lopez-Cuesta, J. M., Billon, L., Garay, H., and Save, M. (2019). Transparent polymer nanocomposites: an overview on their synthesis and advanced properties. *Prog. Polym. Sci.* 89, 133–158. doi:10.1016/j.progpolymsci.2018.10.003

Mallakpour, S., and Behranvand, V. (2016). Nanocomposites based on biosafe nano ZnO and different polymeric matrixes for antibacterial, optical, thermal and mechanical applications. *Eur. Polym. J.* 84, 377–403. doi:10.1016/j.eurpolymj.2016. 09.028

Manabolu Surya, S. B., Nallamalla, S. B., and Amaravathi, C. (2025). Functionalized carbohydrate polymers-based metal nanocomposites for antimicrobial application. $99-118.\ doi:10.1007/978-981-96-2171-2_5$

Matijaković Mlinarić, N., Altenried, S., Selmani, A., Nikolić, J., Učakar, A., Zore, A., et al. (2024). Biocompatible polyelectrolyte multilayers with copper oxide and zinc oxide nanoparticles for inhibiting bacterial growth. *ACS Appl. Nano Mater.* 7 (11), 12550–12563. doi:10.1021/acsanm.4c00981

Motelica, L., Ficai, D., Oprea, O., Ficai, A., Trusca, R. D., Andronescu, E., et al. (2021). Biodegradable alginate films with zno nanoparticles and citronella essential Oil-a novel antimicrobial structure. *Pharmaceutics* 13 (7), 1020. doi:10.3390/pharmaceutics13071020

Nallamalla, S. B., Pradeep, N., Maity, C. K., and Manabolu Surya, S. B. (2025). β-Keto-Enamine-Functionalized nitrogen-rich covalent organic frameworks for metal-free H 2 sensor at room temperature. ACS Appl. Polym. Mater. 7 (14), 9410–9421. doi:10.1021/acsanm.5c01845

Pandey, M., Singh, M., Wasnik, K., Gupta, S., Patra, S., Gupta, P. S., et al. (2021). Targeted and enhanced antimicrobial inhibition of mesoporous ZnO-Ag2O/Ag, ZnO-CuO, and ZnO-SnO2Composite nanoparticles. *ACS Omega* 6 (47), 31615–31631. doi:10.1021/acsomega.1c04139

Paul, S., Sen, B., Basak, N., Chakraborty, N., Bhakat, K., Das, S., et al. (2023). Zn3Sb4O6F6 and KI-Doped Zn3Sb4O6F6: a metal oxyfluoride system for photocatalytic activity, knoevenagel condensation, and bacterial disinfection. *Inorg. Chem.* 62 (2), 1032–1046. doi:10.1021/acs.inorgchem.2c04006

Perfileva, A. I., and Krutovsky, K. V. (2024). Manganese nanoparticles: synthesis, mechanisms of influence on plant resistance to stress, and prospects for application in agricultural chemistry. *J. Agric. Food Chem.* 72 (14), 7564–7585. doi:10.1021/acs.jafc. 3c07350

Rezaei, F. Y., Pircheraghi, G., and Nikbin, V. S. (2024). Antibacterial activity, cell wall damage, and cytotoxicity of zinc oxide nanospheres, nanorods, and nanoflowers. ACS Appl. Nano Mater. 7 (13), 15242–15254. doi:10.1021/acsanm.4c02046

Salama, A., Diab, M. A., Abou-Zeid, R. E., Aljohani, H. A., and Shoueir, K. R. (2018). Crosslinked alginate/silica/zinc oxide nanocomposite: a sustainable material with antibacterial properties. *Compos. Commun.* 7, 7–11. doi:10.1016/j.coco.2017. 11.006

Sánchez-López, P., Hernández-Hernández, K. A., Fuentes Moyado, S., Cadena Nava, R. D., and Smolentseva, E. (2023). Antimicrobial and virus adsorption properties of Y-Zeolite exchanged with silver and zinc cations. ACS Omega. doi:10.1021/acsomega. 3c06462

Sujith Benarzee, N., Kumar, V., and Hussain Reddy, K. (2023). Green synthesis characterization and anti-bacterial activity of neem flowerextract assisted silver nanoparticles. *Karnatak Univ. J. Sci.*, 0075–5168. doi:10.61649/kujos/v54i3.benarzee

Supramaniam, J., Low, D. Y. S., Wong, S. K., Tan, L. T. H., Leo, B. F., Goh, B. H., et al. (2021). Facile synthesis and characterization of palm CNF-ZnO nanocomposites with antibacterial and reinforcing properties. *Int. J. Mol. Sci.* 22 (11), 5781. doi:10.3390/ijms22115781

Tabata, Y. (2000). Tissue engineering. Jpn. J. Artif. Organs 29 (5), 614–615.

Valinton, J. A. A., Kurniawan, A., Jhang, R. H., Pangilinan, C. R., Lee, C. H., and Chen, C. H. (2022). Invisible bactericidal coatings on generic surfaces through a convenient hand spray. *Langmuir* 38 (48), 14909–14917. doi:10.1021/acs.langmuir.2c02604

Varun Kumar, B., and Reddy, K. H. (2023). Synthesis, characterization and antimicrobial activity of novel silver nanoparticles functionalized with nitrogenous ligands. *Inorg. Nano-Metal Chem.* 54, 1127–1136. doi:10.1080/24701556.2023.2165686

Wee, G. (1998). Protein release from alginate matrices. Adv. Drug Deliv. Rev. 31 (3), 267-285. doi:10.1016/s0169-409x(97)00124-5

Wu, J. H., Hu, T. G., Wang, H., Zong, M. H., Wu, H., and Wen, P. (2022). Electrospinning of PLA nanofibers: recent advances and its potential application

for food packaging. J. Agric. Food Chem. 70 (27), 8207-8221. doi:10.1021/acs.jafc. 2c02611

Yan, R., Takahashi, T., Zeng, H., Hosomi, T., Kanai, M., Zhang, G., et al. (2021a). Robust and electrically conductive ZnO thin films and nanostructures: their applications in thermally and chemically harsh environments. *ACS Appl. Electron. Mater.* 3 (7), 2925–2940. doi:10.1021/acsaelm.1c00428

Yan, R., Takahashi, T., Zeng, H., Hosomi, T., Kanai, M., Zhang, G., et al. (2021b). Enhancement of PH tolerance in conductive Al-Doped ZnO nanofilms *via* sequential annealing. *ACS Appl. Electron. Mater.* 3 (2), 955–962. doi:10.1021/acsaelm.0c01052

Zare, M., Zare, M., Butler, J. A., and Ramakrishna, S. (2021). Nanoscience-led antimicrobial surface engineering to prevent infections. *ACS Appl. Nano Mater.* 4 (5), 4269–4283. doi:10.1021/acsanm.1c00466

Zhang, D., Pan, Q., Jia, M., Zhang, X., and Wang, Y. (2021). Three birds with one stone: preventive protection of paper materials by ZnO-PHMB and UV-531 composite systems. *Langmuir* 37 (28), 8445–8454. doi:10.1021/acs.langmuir.1c00770

Zhou, K., Yan, X., Oh, S. J., Padilla-Rivera, G., Kim, H. A., Cropek, D. M., et al. (2023). Hierarchically patterned self-cleaning polymer composites for daytime radiative cooling. *Nano Lett.* 23 (9), 3669–3677. doi:10.1021/acs.nanolett.2c04069